Since January 2020 Elsevier has created a COVID-19 resource centre with free information in English and Mandarin on the novel coronavirus COVID-19. The COVID-19 resource centre is hosted on Elsevier Connect, the company's public news and information website.

Journal of King Saud University – Science 34 (2022) 102296

HOSTED BY

Contents lists available at ScienceDirect

Journal of King Saud University – Science

journal homepage: www.sciencedirect.com

Original article

ZnO-chlorogenic acid nanostructured complex inhibits Covid-19 pathogenesis and increases hydroxychloroquine efficacy

Mosleh M. Abomughaid [a], Mohammed S. Nofal [b], Khaled I. Ghaleb [a], Mohamed G. Seadawy [c], Miral G. AbdEl-Wahab [b], Alaa S. Hegazy [d,e], Doaa A. Ghareeb [e,f,*]

[a] Medical Laboratory Sciences Department, College of Applied Medical Sciences, University of Bisha, Bisha, Saudi Arabia
[b] Center of Excellency for Drug Preclinical Studies (CE-DPS), Pharmaceutical and Fermentation Industries Development Centre, City of Scientific Research and Technological Applications (SRTA-City), New Borg El-Arab, Alexandria, Egypt
[c] Biological Prevention Department, Egyptian Army, Egypt
[d] Medical Laboratories Department, Faculty of Allied Medical Science, Pharos University, Alexandria, Egypt
[e] Bio-screening and Preclinical Trial Lab, Biochemistry Department, Faculty of Science, Alexandria University, Alexandria, Egypt
[f] Biochemistry Department, Faculty of Science, Alexandria University, Alexandria, Egypt

ARTICLE INFO

Article history:
Received 26 March 2022
Revised 2 August 2022
Accepted 25 August 2022
Available online 30 August 2022

Keywords:
VeroE6 toxicity
Plaque assay
Papain-like proteinase
RNA dependent RNA polymerase

ABSTRACT

Objective: The study purpose was to compare the anti- novel coronavirus disease 2019 (COVID-19) property of chlorogenic acid (CGA) and Zinc oxide nanoparticles (ZnO-NP) with the new valid synthesized complex of ZnO /CGA-NPs.
Methods: The facile mixing method was utilized to prepare ZnO/CGA-NPs. The *in vitro* effect of different ZnO/CGA-NPs concentrations on papain-like protease (PL^{pro}) and spike protein- receptor-binding domain (RBD) was measured by ELISA technique. The compounds effects on SARS-CoV2 were determined on viral entry, replication, and assembly by using plaque reduction assay, qPCR, and ELISA techniques. Their individual effects or mixed with hydroxychloroquine (HCQ) on erythrocytes (RBCs) and leukocytes (WBCs) were evaluated by routine cell culture technique. Finally, turbidity and agar well diffusion assays were done to evaluate their antimicrobial properties against *Escherichia. coli*, *klebsila pneumonia, Streptococcus pyogenes*, *Staphylococcus aureus*, and *Candida albicans*.
Results: The results confirmed that the uniformly dispersed ZnO-NPs were converted to aggregated form of ZnO/CGA-NPs upon the addition of CGA. The inhibitory concentration 50 (IC_{50}) of ZnO /CGA-NPs against RBD, angiotensin-converting enzyme 2 (ACE2) and PL^{pro} were 1647.7, 323.3 µg/mL and 38.7 µg/mL, respectively. Also, it inhibited E-gene, RdRp gene, E-protein, and spike protein with an IC_{50} of 0.11, 0.13, 0.48, and 0.37 µg/mL, respectively. It acted as an antimicrobial against all tested organisms with a minimum inhibitory concentration (MIC) of 26 µg/mL. Finally, ZnO/CGA-NPs Complex (0.1 IC_{50}) prevented the cytotoxic effect of HCQ on RBCs and WBC by 92.3 and 90 %, respectively.
Conclusion: ZnO/CGA-NPs Complex can be considered as a new anti- severe acute respiratory syndrome coronavirus 2 (SARS-CoV2) compound.

1. Introduction

Till 30 July 2022 and according to the world health organization (WHO) statics, the pandemic disorder COVID-19 (Zhu et al. 2020) infected 581,304,308 cases from that there were 6,418,377 deaths worldwide. The viral proteins divided into structural protein which are envelop (E), membrane (M), spike (S) and nucleocapsid (N) protein as well as numerous non-structural proteins (NSP). Each one has a central role during virus entry, replication, and transcription. Each protein can be considered an effective drug target where *N*-protein is a drug target to stop viral replication (Jack et al. 2020;

Abbreviations: ACE2, angiotensin-converting enzyme 2; CGA, chlorogenic acids; COVID 19, coronavirus disease 2019; HCQ, hydroxychloroquine; PL^{pro}, papain-like proteinase; RBD, spike protein-receptor binding domain; SARS-CoV-2, severe acute respiratory syndrome coronavirus 2; ZnO, Zinc oxide.

* Corresponding author at: Bio-screening and Preclinical Trial Lab, Biochemistry Department, Faculty of Science, Alexandria University, Alexandria, Egypt.
E-mail address: d.ghareeb@alexu.edu.eg (D.A. Ghareeb).

Peer review under responsibility of King Saud University.

Production and hosting by Elsevier

https://doi.org/10.1016/j.jksus.2022.102296
1018-3647/

Boopathi et al. 2021). Both Spike and furin are targets to prevent the viral entry (Wan et al. 2020; Walls et al. 2020). Several studies reported that about one quarter of COVID-19 patients are co-infected with different microbes such as *Staphylococcus aureus, Streptococcus pneumoniae, and Candida albicans* (Contou et al. 2020; Ghareeb et al. 2021a), therefore the use of an empiric antibiotic is encouraged.

Despite, a few drugs as anti-COVID-19 was approved as anti-COVID 19, the new challenge for scientists is to find out new compounds derived from natural resources to be used as COVID-19 therapeutic agents. Because natural product can kill microbe, prevent the formation of biofilm, work on multitargets (Sharma et al., 2021), beside that it safer and more efficient than several synthetic drugs (Ghareeb et al. 2021b).

The *in vitro* and *in silico* reporters proved that synthetic and natural antioxidants compounds can be used for COVID-19 treatment (Chauhan et al. 2021), such as berberine, curcumin, vitamin C, and caffeic acid (CA). Chlorogenic acids (CGAs), which is CA derivatives, have a wide spectrum of biological activities, including antidiabetic, hypolipidemic, antioxidants, and anti-inflammatory (Prasad et al. 2011). This phenolic acid, that is esters of quinic acid with cinnamic acids, is richly found in green coffee beans as well as coffee (Matei et al. 2012). Recently, Wang et al. (2022) proved that CGA could be a good candidate for COVID-19 treatment as their molecular docking results revealed that CGA binds to several targets such as ACE and interleukin (IL) 6.

It is well known that respiratory infections are associated with zinc deficiency. Zinc oxide (ZnO) nanoparticles (NPs) show antimicrobial activity, inhabiting the replication of different life throttles viral infections and respiratory viral pathogens such as SARS-CoV1 (Liu et al. 2020) due to the ROS production (Sharma et al., 2021). ZnO-NPs can fight viral infections through several mechanisms, including modulating the viral particle entry and fusion, preventing the viral replication, which consequently interferes with translation of viral protein infection (Ghareeb et al. 2021a, Ghareeb et al., 2021b; Hamdi et al. 2021).

Despite, HCQ shows several side effects when used as anti-COVID-19 on clinical trials, it shows *in vitro* anti-COVID-19 properties (Ghareeb et al. 2021a; Infante et al. 2021).

Based on these findings, this work was carried out to investigate the efficacy of ZnO-NPs, CGA and ZnO/CGA-NPs complex as anti-COVID-19, antimicrobial, and hydroxychloroquine (HCQ) toxicity eliminators.

2. Material and methods

2.1. Materials

CGA (>99 purity), Milli-Q water, 3-(4, 5-dimethylthiazol −2-yl)-2, 5-diphenyltetrazolium bromide (MTT), Ethanol and methanol (HPLC grade) were purchased from Sigma Aldrich (Germany). Zinc acetate dihydrates and Sodium hydroxide pellets (Fisher Chemical) were used.

2.2. ZnO nanoparticles and ZnO/CGA complex preparation and characterization

ZnO- NPs with 30 ± 5 nm hexagonal wurtzite structure was synthesized according to Aditya et al. (2018) and Ghareeb et al. (2021a). The facile mixing method was utilized to prepare the ZnO/CGA complex as reported by Belay et al. (2017). Firstly, the dispersed ZnO-NPs in Milli-Q water (225 µg/mL) by ultrasonication for 30 min was mixed with 2.6 mL of 100 µg/mL aqueous chlorogenic acid (CGA) solution and diluted under stirring to achieve a 1:0.5 ZnO:CGA mixture until the cloudy suspension of ZnO-NPs was instantly transformed to pale yellow. The solution was agitated at 25 °C for 2 h before using a freeze dryer to get the ZnO/CGA-dried yellow powder.

The ZnO-NPs and ZnO/CGA-complex spectra were performed at room temperature in the range of 200–500 nm using a UV–vis Spectrophotometer (Thermo Scientific™ Evolution™ 300). A Fourier transform infrared (FTIR, Shimadzu IRTracer-100 FT-IR) spectrophotometer was used to assess the interaction of ZnO and CGA confirmed using a wave number range of 4000–400 cm^{-1}. Finally, the hydrodynamic size, morphology, and the crystalline nature of the ZnO-NPs and ZnO/CGA were measured using Zetasizer Nano ZS (Malvern, Worcestershire, UK), transmission electron microscopy (TEM) (JEOL, JEM 1400, Tokyo, Japan), and (Shimadzu XRD-6100 diffractometer) with a copper source (1.54 Å). Intensity (counts) values were detected in the 2θ range of 10-80°, with 30 mA (current) and 40 kV (tension).

2.3. In silico analysis

Chem Sketch program was used to draw the chemical structure of compounds in MOL format that converted to PDB file by Babel software. PDB of target proteins were obtained from www.rscb.org. Proteins' co-ordinates energy minimization was done by SWISS-PDB VIEWER (SPDBV). Autodock.4 was used to analyze the ligand protein interaction (LPI) where the grid box size was (126 points in x, y and z dimensions), and spacing (0.375 Ã…) while the docking were used by lamarckian genetic algorithm (LGA) at 2,500,000 energy evaluations and the number of run (pose) was 10. The minimum binding energy was calculated by using Cygwin software. Finally, the LPI visualization was carried by the UCSF Chimera software.

2.4. Anti-COVID-19 assays

2.4.1. Determination of compounds inhibitory activity towards papain-like proteinase, spike protein

The inhibitory activities of ZnO-Nps, CGA, ZnO/CGA complex, and HCQ towards papain-like proteinase ((PLpro), Abcam, UK, cat# ab277615) and spike protein-receptor binding domain ((RBD), Abcam, UK, cat# ab273065) were determined according to Tai et al. (2020). While the compounds-ACE-2 binding efficiency was measured according to Ghareeb et al. (2021a).

2.4.2. In vitro VeroE6 toxicity

In a microwell-plate, tested compounds serial dilutions were added to 24 h cultured Vero E6 (30000 cells) then the plate was incubated for another 24 h in a calibrated CO_2 incubator. The viable cells were visualized by MTT assay as described by Ghareeb et al. (2021a). The concentration that demonstrated 50 % cytotoxic effect (50 % cell death, IC50) was calculated from plot that contained % cytotoxicity (((Abs of cell without treatment-Abs of cells with treatment)/ Abs of cell without treatment) *100) on Y axis and sample concentration in X axis. The IC50 was used as the maximum concentration of the tested compound in plaque reduction assay.

2.4.3. Anti-COVID-19 activity (Plaque reduction assay)

The plaque reduction assay was carried out according to standardized published methods Xia et al. (2020), in which the plaques percentage inhibition was recorded as follows;

$$\% \text{ inhibition} = \text{viral count (untreated)} - \frac{\text{viral count treated}}{\text{viral count (untreated)}} \times 100$$

2.4.4. Antiviral activity

In cell culture plate (12wells), the seeded Vero E6 cell was infected with SARS-CoV-2 (provided from chemical warfare, Egyptian Army) at an 0.1 MOI and incubated for 2 h. After changing the media with fresh one containing serial dilutions of tested compounds or without (control), the plate was 3 days incubated at 37 °C in 5 % CO_2. After centrifugation at 600 rpm for 10 min, the cells were scraped and added to 1 mL culture media. The virus was killed by exposing the supernatant and cells to routine UV disinfection protocol for 5 min, followed by cell lysis via sawing and freezing. The cellular RNA was isolated by using Qiagen viral RNA-isolation kit (#52906). cDNA was synthesized by using cDNA synthesis kit (Thermo Scientific, USA). Finally, the viral RdRp gene and E-gene amplification was carried out according to method of Xia et al. (2020). The gene expression was calculated by the -ΔΔCt method.

The spike protein and envelope protein levels were determined by ELISA technique (Xia et al., 2020).

2.5. In vitro bioscreening assays of the tested compounds

2.5.1. In vitro anti-hemolytic activity

The antihemolytic activities of ZnO-NPs, CGA, ZnO/CGA complex, and HCQ was determined as described by Ghareeb et al. (2021a). The effective concentration (EC_{50}) that prevented a 50 % RBC hemolysis was measured in μg/mL by plotting % anti-hemolytic effect (((Abs in absences of treatment-Abs in presence of treatment)/ Abs in absences of treatment) *100) on Y axis and sample concentration in X axis.

2.5.2. In vitro peripheral blood monocytes (PBMCs) cytotoxicity

Rabbit PBMCs were isolated by adding Ficoll media. After centrifugation, the number of viable PBMCs was measured by trypan blue, and then resuspended at 1.0×10^5 cell/mL in RPMI culture medium. 100 μL of cells were cultured for 24 h in calibrated CO_2 (5 % CO_2, and 95 % humidity) then, serial dilutions of each compound (100 μL) were added to the cells, and the cells were re-incubated for an additional 24 h at the same conditions. MTT assay was used to determine the cell viability.

2.5.3. DPPH scavenging activity

The free radical scavenging activity of tested compounds was measured according to Brand-Williams et al. (1995).

2.5.4. Antimicrobial activity

Agar well diffusion and turbidity assays (Kadaikunnan et al. 2015) were used to detect the activity of the compounds against five microbial species *Klebsila pneumonia (ATCC700603),* E. coli (ATCC25922), *Staphylococcus aureus (*ATCC25923), *Streptococcus pyogenes (EMCC1772*), and *Candida albicans* (EMCC105). The minimum inhibitory concentration (MIC) was calculated for each compound tested.

2.6. Determination of in vitro HCQ toxicity elimination

For red blood cells, 100 μL of RBCs suspension (1 %) was mixed and incubated at 37 °C for 30 min with the concentration of tested compound (450 μL) that demonstrated the lowest hemolytic effect. Then, 450 μL of 27.5 μg/mL HCQ was added then this mixture was

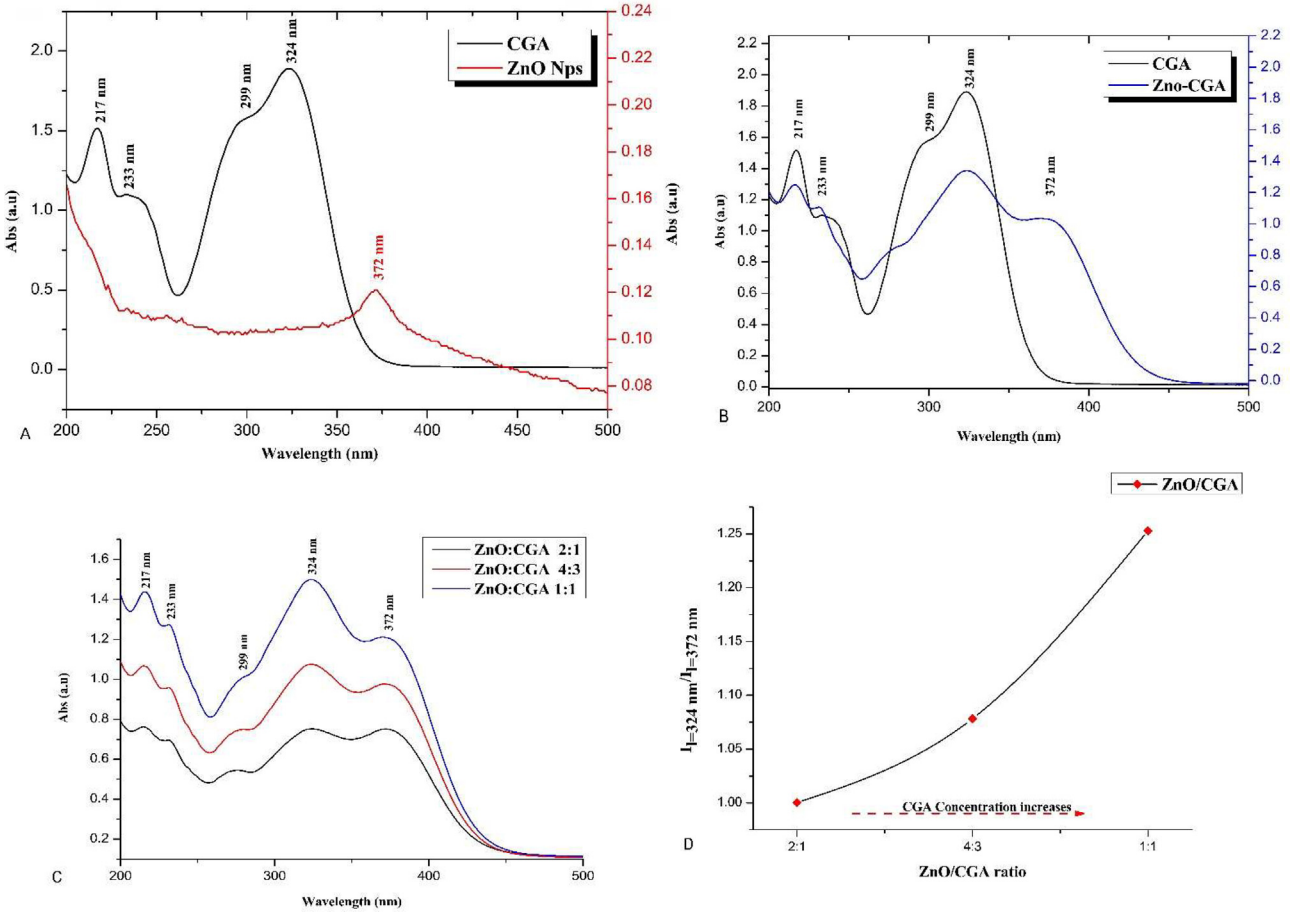

Fig. 1. The UV–vis absorption spectrum of (A) CGA vs ZnO, (B) CGA vs ZnO/CGA, (C) ZnO vs CGA and ZnO/CGA, and (D) effect of excess CGA to constant ZnO-Nps.

re-incubated for another 30 min. the absorptance of the supernatant was measured at 540 nm. Finally, the percentage of hemolysis was calculated.

For white blood cells (WBCs), the WBCs were isolated from 10 mL of blood, and then the palette was suspended in 10-fold resuspended in 1 mL culture RPMI (Dagur & McCoy 2015). The viable cells were then diluted to a concentration of 1×10^5 cell/mL in culture RPMI 1640 medium for 24 h in a CO_2 incubator at standardized conditions. Following that, 100 µL of different concentrations of tested compounds were added alone or in the presence of HCQ concentration (that yield 50 % cell death) for 24 h in a CO_2 incubator under standardized conditions. The cell proliferation was measured by MTT assay.

2.7. Statistical analyses

Data were expressed as means and standard deviations. The significant difference among groups was set at $p < 0.05$ using ANOVA, *post hoc* LSD test, and multiple comparison test in SPSS software package version 20.0 (Armonk, NY: IBM Corp).

3. Results

In the case of ZnO-NPs, only one absorption band at 372 nm was detected while four characteristic peaks for CGA at 217, 233, 299, and 324 nm (Fig. 1A) was found. The mixing of CGA with ZnO-Nps (Fig. 1B and 1C) showed hypochromic effects in the absorbance pattern which was associated with the appearance of the characteristic absorption peak of metal-phenolate at 372 nm. The addition of excess CGA to constant ZnO-Nps which calculated by $I_{\lambda=324nm}/I_{\lambda=372nm}$ ratio (Fig. 1D) indicated that the addition of CGA after stoichiometry of ZnO/CGA = 2 was ineffective as the intensity of the CGA characteristic peak 324 nm was progressively increased while the metal-phenolate peak at 372 nm of ZnO/CGA remained constant.

The IR spectra (Fig. 2A) showed that in the ZnO/CGA spectrum, the characteristic Zn-O absorption bands of ZnO-Nps were observed at 428 cm^{-1}, while the Zn-OH absorption band at 499 cm^{-1} was disappeared, moreover, almost all CGA characteristic absorption bands were presented. TEM images showed that the uniformly-highly dispersed particles of ZnO-NPs (30 ± 5 nm) (Fig. 2B) were converted into agglomerated clusters in ZnO/CGA-Nps (Fig. 2C) due to the presence of CGA on the surface of ZnO-NPs.

The *in silico* study presented in Fig. 3 and Table 1 shows that ZnO/CGA had different ligand protein interaction (LPI) than both parents, where it binds with PL^{pro} by two hydrogen bonds with Gln 270 and Tyr 274 and several hydrophobic interactions. This LPI showed the lowest binding energy (−17.8 kj) and estimated Ki (89.1 fM). Despite both CGA and ZnO-NPs bind with spike protein with hydrogen bonds, the ZnO/CGA complex binds with the protein through hydrophobic interactions only and it shows the lowest binding energy (−15.55 kj) and estimated Ki (4.01 nM). Finally, ZnO/CGA complex binds with RBD by five hydrogen bonds at LEU 91, LYS 94, ASP 206, ASN 210, and GLY 395 and it shows the lowest binding energy (-10.99 kj) and estimated Ki (8.82 nM). Table 2 shows that all tested compounds inhibited PL^{pro} in a concentration-dependent manner where the highest inhibitory effect was shown in the case of ZnO/CGA complex followed by ZnO-NPs, then HCQ, and finally CGA where the relative IC50s were 38.67, 48.5, 270.3, and 3571.4 µg/mL, respectively. All tested

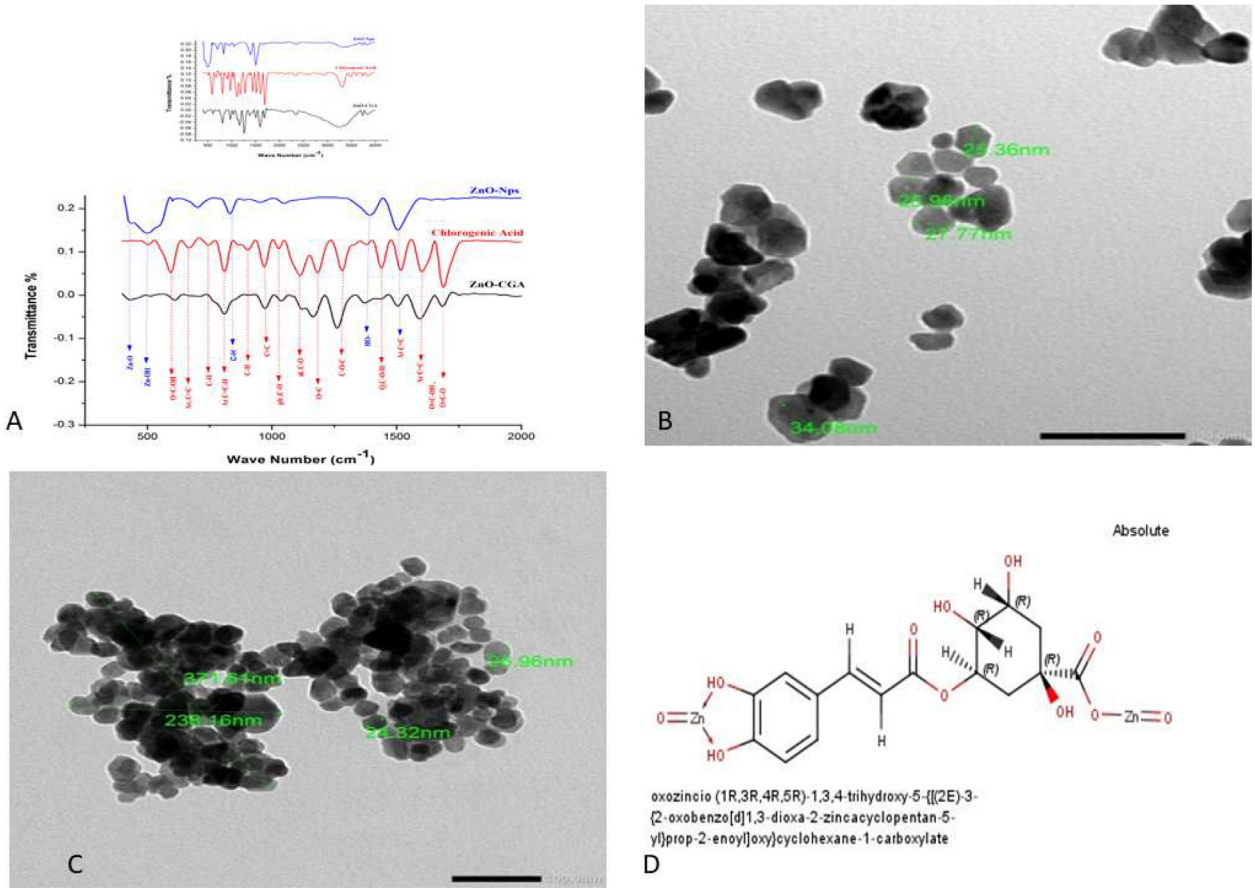

Fig. 2. (A) The Fourier transform infrared (FTIR) spectrum of ZnO-Nps, CGA, and ZnO/CGA complex and (B and C, the magnification power was 100 nm) TEM and analysis of ZnO-NPs and ZnO/CGA and (D) The proposed structure of ZnO/CGA complex.

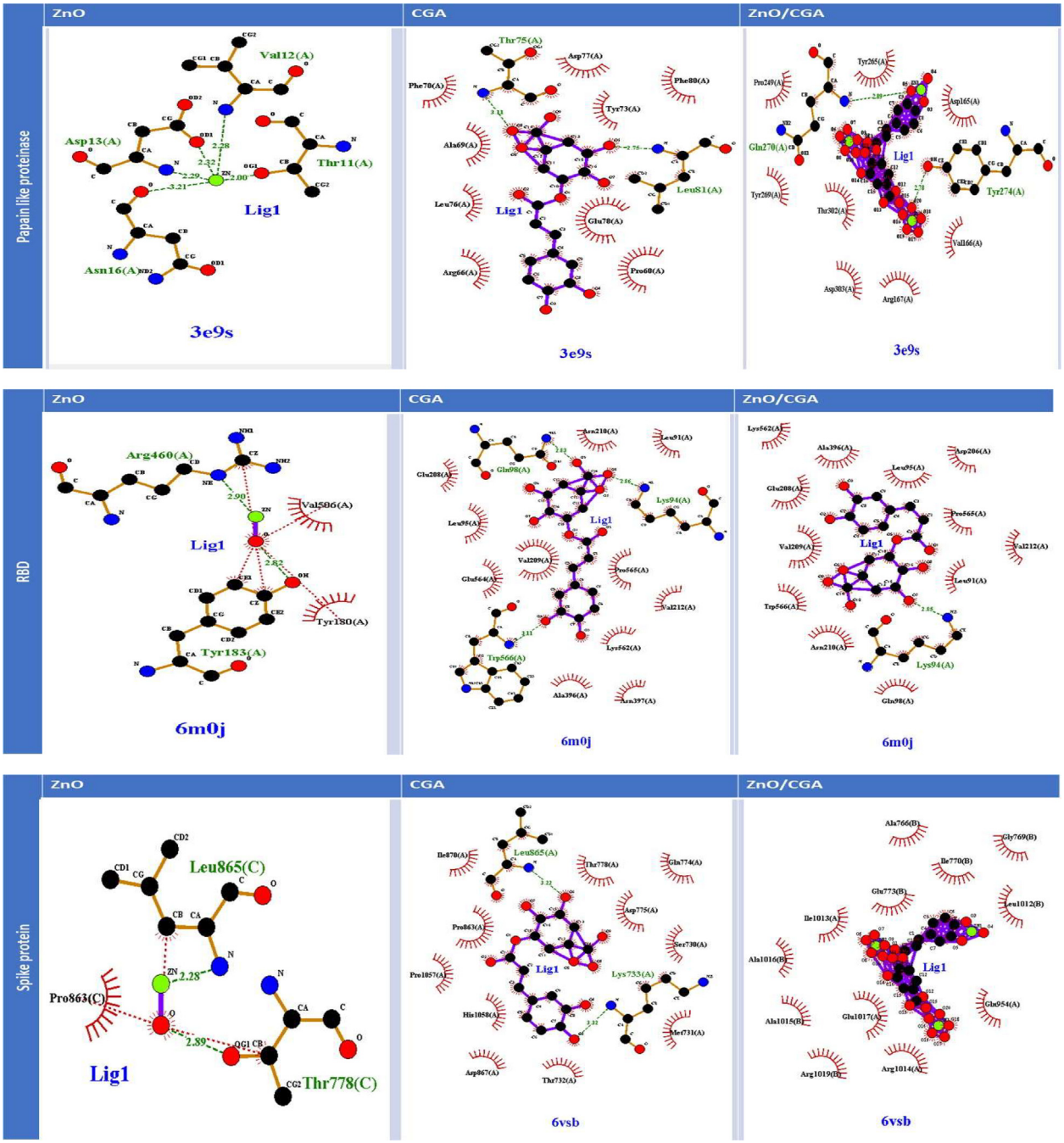

Fig. 3. Molecular docking and LigPlus analysis illustrating the interaction between ZnO-NPs, CGA, and ZnO/CGA and the studied proteins (papain-like proteinase, spike protein, and spike protein receptor-binding domain).

compounds had ACE2 binding affinity and increased the formation of the RBD-ACE2 complex.

In accordance with the previous data, Table 3 shows that all tested compounds acted as anti-SARS-CoV2 where the highest antiviral effect was shown in the case of ZnO/CGA complex followed by CGA and HCQ and finally ZnO-Nps. The obtained data confirmed that these compounds could be considered potent antiviral candidates because the obtained EC50s (effective antiviral concentration 50) for all tested compounds were lower than their IC50s (Vero E6 inhibitory concentration 50).

Interestingly, our data which is represented in Table 4 confirmed that ZnO-NPs, CGA, and ZnO/CGA complex inhibited the ORF, E- and RdRp-gene expression in a concentration-dependent manner where the ZnO/CGA complex showed the maximum gene down-regulation patterns. In accordance with gene expression data, the ZnO/CGA complex showed the maximum inhibition E-protein and spike protein pattern.

Table 5 proves that CGA was the safest compound toward RBC, PBMCs and WBCs where it showed the highest IC_{50} followed by ZnO/CGA complex, ZnO-NPs and finally HCQ. In addition, the ZnO/CGA complex presented the highest antioxidants capacity followed by CGA, HCQ, and finally ZnO-NPs.

Table 6 shows that all tested compounds acting as anti- *Klebsila pneumonia, Staphylococcus aureus, Streptococcus pyogenes,* and *Candida albicans* where the highest antimicrobial effect was shown in the case of ZnO/CGA complex.

Table 1
Docking results of the tested compounds with papain-like proteinase, spike protein, and spike protein receptor-binding domain.

Parameters	CGA	ZnO	ZnO/ CGA	Reference inhibitor
pH		6.75		
PAPAIN-LIKE PROTEINASE				
Name of Reference inhibitor				**5-Amino-2-Methyl-N-[(1r)-1-Naphthalen-1-Ylethyl]benzamide**
Hydrogen bond	LIG 1O-THR 75.A OG1 LIG 1O-LEU 76.A O LIG 1O-ASP 77.A O LIG 1O-GLU 78.A O LEU 81.A *N*-LIG 1O	No hydrogen bond	LIG 1O- Gln 270. A N LIG 1O- Tyr 274. A OH Hydrophobic interaction	LIG 1 N /A GLU 168 OE1 no hydrogen 2.647 N/A LIG 1 N /A GLU 180 OE2 no hydrogen 3.064 N/A
Binding energy	−10.58	−2.77	−17.8	−3.98
Estimated Ki	17.49 nM	9.28 mM	89.10 fM	1.21 mM
Reference RMSD	36.54	32.56	44.24	62.53
SPIKE PROTEIN				
Name of Reference inhibitor				**Geraniin**
Hydrogen bond	LIG 1O-MET 731.A O LIG 1O-ASP 775.A OD1 LIG 1O-LEU 865.A O LYS 733.A *N*-LIG 1O	LIG1O-ASP775.C OD1 LIG1O-THR778.C-OG1	No hydrogen bond Hydrophobic interaction	LIG O/Gln 314 N
Binding energy	−9.77	−2.74	−15.55	−16.68
Estimated Ki	69.39 nM	9880 uM	4.01 pM	595.11 fM
Reference RMSD	385.4	385.03	378.33	263.02
SPIKE RECEPTOR-BINDING DOMAIN				
Name of Reference inhibitor				**Amentoflavone**
Hydrogen bond	LIG 1O-GLU 208.A O LYS 94.A NZ-LIG 1O GLN 98.A NE2-LIG 1O TRP 566.A N- LIG 1O	LIGO-TYR183.A OH LIGO-VAL506.A O	LIG 1O-LEU 91.A O LIG 1O-ASP 206.A O LIG 1O-GLY 395.A O LYS 94.A NZ-LIG 1O ASN 210.A ND2-LIG 1O	ASN 210 N—LIG O
Binding energy	−10.34	−2.31	−10.99	−12.17
Estimated Ki	26.30 nM	20,180 uM	8.82 nM	1.19 nM
Reference RMSD	50.17	66.63	55.6	60.26

Table 2
The inhibitory/binding effect of the tested compound on papain-like proteinase, Spike protein receptor binding domine and ACE2.

Groups	Concentration μg/mL	PL^{pro} inhibition %	SP- RBD-ACE2 complex formation fold	ACE-2 Binding %
ZnO	104	71.06 ± 1.3^{e}	20.25 ± 0.5^{e}	16.4 ± 0.9^{d}
	52	62.2 ± 0.90^{d}	13.375 ± 0.3^{d}	15.6 ± 0.7^{d}
	26	45.6 ± 1.1^{c}	6.625 ± 0.2^{c}	13.1 ± 1.3^{c}
	13	35.31 ± 0.77^{b}	3.5 ± 0.3^{b}	10.7 ± 0.8^{b}
	6.5	22.5 ± 0.12^{a}	0.5 ± 0.02^{a}	8.2 ± 0.08^{a}
IC50 (μg/mL)		**48.5**	**256.8**	**317.1**
CGA	1000	14.5 ± 0.9^{c}	14.25 ± 0.5^{d}	18.3 ± 1.2^{b}
	500	13.6 ± 1.1^{c}	13.875 ± 0.3^{d}	18.1 ± 2.1^{b}
	250	11.2 ± 0.7^{b}	4.375 ± 0.1^{c}	17.2 ± 1.1^{ab}
	125	10.6 ± 1.01^{b}	1 ± 0.01^{b}	16.4 ± 1.1^{a}
	62.5	6.9 ± 0.4^{a}	0.75 ± 0.002^{a}	14.8 ± 1.2^{a}
IC50 (μg/mL)		**3571.4**	**3508.8**	**2732.2**
ZnO/CGA	156.5	80.3 ± 1.9^{d}	4.75 ± 0.2^{e}	24.2 ± 0.1^{e}
	78.25	65.1 ± 2.8^{c}	1.625 ± 0.07^{d}	17.1 ± 0.2^{d}
	39.215	50.7 ± 3.4^{b}	0.625 ± 0.003^{c}	15.6 ± 0.1^{c}
	19.563	45.6 ± 2.1^{b}	0.375 ± 0.007^{b}	11.5 ± 0.07^{b}
	9.782	38.6 ± 1.2^{a}	0.01 ± 0.001^{a}	9.2 ± 0.05^{a}
IC50 (μg/mL)		**38.67**	**1647.4**	**323.3**
HCQ	200	37 ± 0.42^{e}	0.5 ± 0.001^{d}	15.6 ± 1.4^{b}
	100	30 ± 0.23^{d}	0.5 ± 0.001^{d}	14.8 ± 0.9^{b}
	50	22.5 ± 0.15^{c}	0.375 ± 0.003^{c}	14.5 ± 0.8^{b}
	25	11.2 ± 0.39^{b}	0.25 ± 0.001^{b}	13.8 ± 1.1^{b}
	12.5	8.1 ± 0.74^{a}	0.125 ± 0.007^{a}	9.02 ± 0.5^{a}
IC50 (μg/mL)		**270.3**	**20,000**	**641.03**

The results are mean ± SD of three replicas., means in the same column with different superscripts letters are significantly different at $p < 0.05$, where a is the lowest means and d is the highest one.

Table 3
Antiviral Activity of the tested compounds by using *in vitro* Vero E6 toxicity and plaque reduction assay against SARS-CoV2.

	Vero E6 IC50 (μg/mL)	Reduction %	Dosage (μg/mL)	Anti-SARS CoV2 EC50 (μg/mL)	EC50/IC50 %
CGA	23.6 ± 1.2^{d}	76 ± 1.9^{b}	15.4 ± 0.21^{c}	4.9 ± 0.021^{d}	21 ± 0.9^{b}
ZnO	12.6 ± 0.42^{c}	67.5 ± 1.2^{a}	5.5 ± 0.41^{b}	4.11 ± 0.012^{c}	33 ± 1.2^{d}
ZnO/CGA	1.65 ± 0.003^{a}	80 ± 3.4^{c}	1.56 ± 0.0002^{a}	0.312 ± 0.002^{a}	19 ± 0.78^{a}
HCQ	1.4 ± 0.1^{b}	76 ± 2.5^{b}	1.1 ± 0.13^{a}	0.385 ± 0.01^{b}	28 ± 1.7^{c}

The results are mean ± SD of three replicas., means in the same column with different superscripts letters are significantly different at $p < 0.05$, where a is the lowest means and d is the highest one.

Table 4
Effect of tested compounds on SARS-CoV2 gene expression and protein levels.

Groups	Concentration (μg/mL)	ORF gene expression	ORF gene downregulation %	E-gene expression	E-gene downregulation %	RdRp expression	RdRp down regulation %	E protein inhibition %	Spike protein inhibition %
ZnO	5.48	0.15 ± 0.001^{a}	85.29 ± 1.1^{c}	0.73E^{-05} ± 0.1 E^{-06a}	99.99 ± 3.6^{b}	0.001 ± 0.0001^{a}	99.9 ± 3.8^{a}	85.71 ± 7.1^{c}	83.33 ± 3.1^{d}
	2.74	0.18 ± 0.002^{b}	81.96 ± 1.6^{c}	3.36 E^{-05} ± 0.1 E^{-06b}	99.99 ± 1.2^{b}	0.018 ± 0.005^{b}	98.2 ± 4.1^{a}	78.57 ± 3.6^{b}	88.89 ± 2.1^{c}
	1.37	0.37 ± 0.001^{c}	62.63 ± 1.4^{b}	5.36 E^{-05} ± 0.1 E^{-06c}	99.99 ± 3.1^{b}	0.019 ± 0.0002^{b}	98.1 ± 3.1^{a}	71.43 ± 1.8^{b}	76.67 ± 3.6^{b}
	0.685	0.47 ± 0.01^{d}	53.35 ± 0.9^{a}	7.36E^{-05} ± 0.1 E^{-06d}	89.78 ± 2.1^{a}	0.028 ± 0.0001^{c}	97.2 ± 2.3^{a}	64.29 ± 2.4^{a}	67.78 ± 1.8^{a}
IC50	μg/mL		**0.641**		**0.38**		**0.24**	**0.365**	**0.51**
CGA	10	0.04 ± 0.0001^{a}	95.99 ± 2.8^{d}	1 E^{-04} ± 0.1 E^{-04a}	99.99 ± 1.8^{a}	0.001 ± 0.1 E^{-05b}	99.89 ± 3.9^{a}	92.5 ± 7.9^{d}	91.66 ± 3.2^{d}
	5	0.096 ± 0.0001^{b}	90.33 ± 3.1^{c}	2 E^{-04} ± 0.1 E^{-04b}	99.97 ± 1.6^{a}	0.0011 ± 1.1 E^{-05b}	99.89 ± 5.2^{a}	87.5 ± 6.4^{c}	83.33 ± 1.3^{c}
	2.5	0.11 ± 0.002^{c}	88.88 ± 2.1^{b}	2 E^{-04} ± 0.1 E^{-04b}	99.97 ± 1.7^{a}	0.0029 ± 1.1 E^{-06c}	99.715 ± 1.2^{a}	75 ± 4.8^{b}	50 ± 0.9b
	1.25	0.13 ± 0.001^{d}	87.7 ± 1.1^{a}	2 E^{-03} ± 0.1 E^{-04d}	99.8 ± 0.9^{a}	0.0033 ± 0.1 E^{-05d}	99.67 ± 1.4^{a}	50 ± 3.6^{a}	25 ± 0.8^{a}
IC 50	μg/mL		**0.71**		**0.63**		**0.63**	**1.25**	**2.5**
ZnO/	CGA	1.565	2.5E^{-05} ± 0.00001^{a}	99.99 ± 1.9^{d}	0.003 ± 0.0001^{a}	99.7 ± 1.4^{d}	1.52E^{-05} ± 0.1E^{-06a}	99.99 ± 1.8^{b}	96 ± 7.8^{c}
	93.3 ± 3.6^{d}								
	0.783	0.015 ± 0.0001^{b}	98.5 ± 2.8^{c}	0.078 ± 0.0001^{b}	92.2 ± 0.1^{c}	0.001 ± 2.3 E^{-06b}	99.89 ± 7.8^{b}	80 ± 6.3^{b}	80 ± 2.7^{c}
	0.391	0.88 ± 0.0001^{c}	11.7 ± 0.03^{b}	0.1 ± 0.001^{c}	90 ± 0.2^{b}	0.001 ± 1.1 E^{-06b}	99.89 ± 3.7^{b}	40 ± 1.5^{a}	53.3 ± 3.1^{b}
0.195	0.93 ± 0.001^{d}	6.7 ± 0.01^{a}	0.14 ± 0.001^{d}	86.03 ± 1.8^{a}	0.234 ± 0.001^{b}	76.67 ± 6.1^{a}	40 ± 2.1^{a}	40 ± 0.9^{a}	
IC 50	μg/mL		**0.53**		**0.11**		**0.13**	**0.48**	**0.37**

The results are mean ± SD of three replicas., means in the same column with different superscripts letters are significantly different at $p < 0.05$, where a is the lowest means and e is the highest one.

Table 5
The antioxidants and RBCs and PBMCs Cytotoxic IC50 of tested compounds.

	RBC IC50 (μg/mL)	PBMC	WBC	Antioxidants
CGA	370.83 ± 12.3^{c}	235 ± 17.8^{c}	655 ± 12.5^{d}	250 ± 10.8^{b}
ZnO	41.67 ± 2.31^{b}	64 ± 0.5^{b}	25 ± 1.1^{b}	439 ± 18.9^{d}
ZnO/CGA	372.15 + 9.4^{c}	230 + 2.01^{c}	395 ± 3.5^{c}	78 ± 1.3^{a}
HCQ	24.55 ± 0.8^{a}	53.2 ± 0.05^{a}	20 ± 1.23^{a}	352 ± 17.8^{c}

The results are mean ± SD of three replicas., means in the same column with different superscripts letters are significantly different at $p < 0.05$, where a is the lowest means and d is the highest one.

Table 7 showed that ZnO-NPs prevented the HCQ hemolytic effect by 82.9 % and increased the WBC viability by 5.6fold while CGA decreased hemolysis by 93 % and increased WBC viability by 9.2fold and finally the ZnO/CGA complex decreased RBCs hemolysis by 92.3 % and increased the WBC viability by 9.7fold.

4. Discussion

This study was aimed to synthesize a ZnO/CGA complex then investigate its efficacy as anti-COVID-19, antimicrobial, and eliminator of hydroxychloroquine (HCQ) toxicity in comparing to its parents' efficiencies.

The characterization data prove the synthesis of a new ZnO/CGA complex that can block the viral entry, replication, and assembly. Besides that, it is considered a potent antioxidant and antimicrobial and it could be used in combination with HCQ as adjuvant therapy. ZnO-NPs had one while CGA UV-spectrum showed four characteristic peaks producing from the Pi transitions that occurred in double bond and the aromatic ring frame (Kalinowska et al. 2020). Moreover, the addition of CGA to ZnO-NPs produced hypochromic effect which indicated the adsorption of CGA onto the ZnO-Nps surface by forming interaction between phenolic catecholate and carboxylate group of CGA with Zn (Kalinowska et al. 2020). The IR absorption spectra indicated the adsorption of CGA on the ZnO-Nps surface. The characteristic

Table 6
Antimicrobial activity using agar well diffusion and turbidity assays.

	Agar well diffusion assay				Turbidity assay			
Concentrations of the tested compounds	Inhibition zone diameter (mm)**			MIC (μg/mL)	Percent of inhibition (%)			MIC (μg/mL)
	100 %	50 %	25 %		100 %	50 %	25 %	
Gram negative Bacteria								
klebsila pneumonia ATCC700603								
ZnO-NPs	11 ± 0.0	ND	ND	104	65.87 ± 0.0	61.84 ± 0.0	44.13 ± 0.0	26
CGA	ND	ND	ND	ND	87.38 ± 0.0	71.32 ± 0.0	58.21 ± 0.0	13
ZnO/CGA	35 ± 0.0	ND	ND	104	88.23 ± 0.0	77.66 ± 0.0	65.11 ± 0.0	26
Positive control (Amoxicillin 0.1 %)	35 ± 0.0				92.48 ± 0.0			
Gram positive Bacteria								
Staphylococcus aureus ATCC25923								
ZnO-NPs	17 ± 0.0	ND	ND	104	87.77 ± 0.0	33.24 ± 0.0	8.09 ± 0.0	26
CGA	ND	ND	ND	ND	61.34 ± 0.0	59.81 ± 0.0	40.37 ± 0.0	13
ZnO/CGA	ND	ND	ND	ND	74.39 ± 0.0	61.88 ± 0.0	50.95 ± 0.0	26
Positive control (Amoxicillin 0.1 %)	25 ± 0.0				95.51 ± 0.0			
Streptococcus pyogenes EMCC1772								
ZnO-NPs	12 ± 0.0	ND	ND	104	68.31 ± 0.0	50.85 ± 0.0	41.49 ± 0.0	26
CGA	ND	ND	ND	ND	68.85 ± 0.0	60.12 ± 0.0	41.53 ± 0.0	13
ZnO/CGA	32 ± 0.0	20 ± 0.0	ND	52	69.95 ± 0.0	63.93 ± 0.0	59.65 ± 0.0	26
Positive control (Amoxicillin 0.1 %)	35 ± 0.0				80.98 ± 0.0			
Yeast								
Candida albicans EMCC105								
ZnO-NPs	30 ± 0.0	25 ± 0.0	20 ± 0.0	26	25.00 ± 0.0	23.44 ± 0.0	20.31 ± 0.0	26
CGA	ND	ND	ND	ND	34.26 ± 0.0	33.04 ± 0.0	17.52 ± 0.0	13
ZnO/CGA	ND	ND	ND	ND	83.15 ± 0.0	65.08 ± 0.0	63.30 ± 0.0	26
Positive control (Fluconazole 0.1 %)	40 ± 0.0				94.14 ± 0.0			

*Diameter includes 5 mm well diameter.
- ND; Not detected.
- MIC; Minimum inhibition concentration.

Table 7
Effect of the tested compounds on HCQ induced RBC hemolysis and WBC cytotoxicity.

Compounds	RBC hemolysis		WBC cytotoxicity	
	Concentration (μg/mL)	Hemolytic (%)	Concentration (μg/mL)	Viability (%)
ZnO	4.1	5.88 ± 0.002^{e}	2.5	53 ± 1.3^{c}
CGA	37	3.52 ± 0.01^{a}	65.5	57 ± 1.3^{c}
ZnO/CGA	37	4.08 ± 0.03^{c}	19.5	57 ± 2.8^{c}
+ve Control (HCQ)	24.5	56 ± 1.3 ^{g}	20	6 ± 0.04^{a}
HCQ + ZnO	24.5 + 4.1	9.6 ± 0.002^{f}	200 + 2.5	34 ± 2.3^{b}
HCQ + CGA	24.5 + 37	3.76 ± 0.05^{b}	200 + 62.5	55 ± 3.7^{c}
HCQ + ZnO/CGA	24.5 + 37	4.32 ± 0.07^{d}	200 + 19.5	58 ± 2.9^{c}

The results are mean ± SD of three replicas., means in the same column with different superscripts letters are significantly different at $p < 0.05$, where a is the lowest means and g is the highest one. Note, the concentration of ZnO-NPs, CGA and ZnO/CGA were 1/10 of IC50s while HCQ concentration was IC50.

CGA absorption bands (667, 809, 1516, and 1600 cm) were attributed to the aromatic ring (Kalinowska et al. 2020). Several alterations had been noticed in ZnO/CGA complex where the redshift intensity was reduced to lower wave numbers (1506 and 1592 cm^{-1}) and the vibration mode of the quinic ring C-OH peak (1438 cm^{-1}) was lost. This could be due to the enrollment quinic ring C-OH in the formation of hydrogen bonds with ZnO surface –OH which also indicated by the band boarding at 3304 cm^{-1} which is specific for the OH group. There were a forceful reduction with the redshift in both the C═O functional group stretching of ester bond band (1687 cm^{-1}) and the C═O carboxyl functional groups stretching band (1183 cm^{-1}) to 1682 and 1165 cm^{-1} which may be suggested that the carboxylate anion may be involved in coordination with zinc (Kalinowska et al. 2020). The the C—O—C stretching vibration in ester bond band (1282 cm^{-1}) has appeared with slightly higher intensity and redshift to 1261 cm^{-1}, the bands of the C—O phenolic and alcoholic stretching (1113 and 1027 cm^{-1}, respectively) were forcibly reduced with the blueshift to 1120 and 1037 cm^{-1}, respectively, indicating that CGA interacted with the surface of ZnO-Nps and ZnO/CGA ground state complex was formed. Altogether, these spectra indicate that CGA interacted with ZnO-NPs by noncovalent bonds. In accordance, the proposed structure of the ZnO/CGA complex was sketched and checked by Chemaxon Marvin sketch software (Fig. 2D).

It is reported that CGA prevents the early stages of the viral infection during virus growth, moreover, it acts as anti-Herpes Simplex Virus I and HCoV-NL63 (Yu et al. 2020; Weng et al. 2019). The obtained results confirmed that the parents and the newly formed complex ZnO/CGA are acting as anti-SARS-CoV2 activity as they increased the cellular pH which leads to endosomal pathway (Xia et al. 2020). The parents and their complex uncompetitively inhibited the binding between RBD and ACE2 through the formation of hydrogen bonds and hydrophobic interaction with RBD that alters the ACE2 active site-specificity to the substrate (Chandel et al. 2020). In this type of inhibition ZnO/CGA binds with enzyme allosteric site and with active site leading to the formation of inactive enzyme-substrate-inhibitor complex. In agreement with these results, the docking study of Yu et al. (2020) proved that CGA interacts with ACE2 at position Gln42 andAsp38 which prevented the ACE2 attachment with S protein. Also, Adem et al. (2021) *in silico* results indicated that CGA interacts with main-proteinase, S proteins subunits and endoribonuclease. Furthermore, ZnO/CGA complex downregulated and inhibited several viral proteins PL^{pro}, RdRp, E and spike proteins which lead to viral replication inhibition. Moreover, CGA binds to cellular heat shock protein A5 which is receptor for COVID-19 (Elfiky, 2021).

Our results indicate that the ZnO/CGA complex binds PL^{pro} active site Gln270 and Tyr274 (Báez-Santos et al. 2015) also it

binds to the ubiquitin-like domine 2 (UL2) (amino acids 75–88) *N*-terminal of PL^{pro} which is linked to the catalytic site. UL2 blocks the formation of the interferon pathway (Shin et al. 2020) therefore our tested compounds could be reduced the viral replication through stimulation of the antiviral interferon pathway.

The toxicity of a new compound must be detected *in vitro* on different normal cells such as WBC, RBC, and fibroblast (Deore et al. 2019). It is known that compounds that acting as antioxidants could be used as adjuvant therapy during COVID-19 infection to decrease the oxidative stress and cytokines storm (Soto et al. 2020). ZnO/CGA complex had the highest antioxidants property. Despite, ZnO-NPs increased cellular oxidative stress, CGA acts as a potent antioxidant, anticancer (Moon et al. 2017and anti-inflammatory (Al-Hatamleh et al. 2020). We must notice that the concentration of ZnO-NPs in this complex is lower than the recommended doses about 15folds, which indicated the elimination of cytotoxic effect of ZnO-NPs (Sharma et al., 2021).

Some COVID-19 infected people had bacterial infection, and this is the reason for the administration of antibiotics for these patients (Contou et al. 2020). All tested compounds had inhibitory ability toward *Klebsila pneumonia, Staphylococcus aureus, Streptococcus pyogenes,* and *Candida albicans*. CGA inhibits bacterial arginase and agmatinase and viral neuraminidase (Moon et al. 2017). CGA is also acting as anti- *Streptococcus pneumoniae* by inhibiting neuraminidase (Guan et al. 2020).

Despite, the presence of HCQ in COVID-19 therapeutic protocol is controversial (Risch 2020) due to associated side effects (Barnabas et al. 2021), it has anti-inflammatory and anti-SARSCoV2 properties. Therefore, we measured the protective effect of tested compounds on RBC hemolysis and WBC destruction by HCQ, and the results proved that ZnO /CGA protects the cells that could be due to the antioxidant and anti-inflammatory properties of CGA (Moon et al. 2017).

5. Conclusion

ZnO/CGA-NPs Complex was successfully prepared by facile mixing method. Where, CGA molecules are interacted by non-covalent interaction on ZnO-Nps surface that formed the ground-state complex. Nano-ZnO /CGA complex exhibited anti-COVID-19 properties as it inhibited several steps in virus lifecycle where it blocked RBD and bind with ACE2 (viral entry targets) Also, it blocked virus replication by inhibiting PL^{pro} and RdRp. This comples is a very potent antimicrobial agent against respiratory tract pathogens. Finally, ZnO/CGA-NPs Complex could be used to eliminate the HCQ associated toxicity.

Declaration of Competing Interest

The authors declare that they have no known competing financial interests or personal relationships that could have appeared to influence the work reported in this paper.

Acknowledgments

The Deanship of Scientific Research, College of Applied medical sciences, University of Bisha, Kingdom of Saudi Arabia has funded this work through the COVID-19 initiative project under the grant (UB-COVID-14-1441).

Appendix A. Supplementary data

Supplementary data to this article can be found online at https://doi.org/10.1016/j.jksus.2022.102296.

References

Adem, Ş., Eyupoglu, V., Sarfraz, I., Rasul, A., Zahoor, A.F., Ali, M., Abdalla, M., Ibrahim, I.M., Elfiky, A.A., 2021. Caffeic acid derivatives (CAFDs) as inhibitors of SARS-CoV-2: CAFDs-based functional foods as a potential alternative approach to combat COVID-19. Phytomedicine. 85, 153310–153326.

Aditya, A., Chattopadhyay, S., Gupta, N., Alam, S., Veedu, A.P., Pal, M., Singh, A., Santhiya, D., Ansari, K.M., Ganguli, M., 2018. ZnO nanoparticles modified with an amphipathic peptide show improved photoprotection in skin. ACS Appl. Mater. Interfaces. 11 (1), 56–72.

Al-Hatamleh, M.A., Hatmal, M.M., Sattar, K., Ahmad, S., Mustafa, M.Z., Bittencourt, M.D., Mohamud, R., 2020. Antiviral and immunomodulatory effects of phytochemicals from honey against COVID-19: Potential mechanisms of action and future directions. Molecules. 25, 5017–5039.

Báez-Santos, Y.M., John, S.E., Mesecar, A.D., 2015. The SARS-coronavirus papain-like protease: structure, function and inhibition by designed antiviral compounds. Antiviral Res. 115, 21–38.

Barnabas, R.V., Brown, E.R., Bershteyn, A., Stankiewicz Karita, H.C., Johnston, C., Thorpe, L.E., Kottkamp, A., Neuzil, K.M., Laufer, M.K., Deming, M., Paasche-Orlow, M.K., Kissinger, P.J., Luk, A., Paolino, K., Landovitz, R.J., Hoffman, R., Schaafsma, T.T., Krows, M.L., Thomas, K.K., Morrison, S., Haugen, H.S., Kidoguchi, L., Wener, M., Greninger, A.L., Huang, M.-L., Jerome, K.R., Wald, A., Celum, C., Chu, H.Y., Baeten, J.M., 2021. Hydroxychloroquine as postexposure prophylaxis to prevent severe acute respiratory syndrome coronavirus 2 infection: a randomized trial. Ann. Intern. Med. 174 (3), 344–352.

Boopathi, S., Poma, A.B., Kolandaivel, P., 2021. Novel 2019 coronavirus structure, mechanism of action, antiviral drug promises and rule out against its treatment. J. Biomol. Struct. Dyn. 39, 3409–3418.

Brand-Williams, W., Cuvelier, M.E., Berset, C.L., 1995. Use of a free radical method to evaluate antioxidant activity. LWT. 28 (1), 25–30.

Chandel, V., Sharma, P.P., Raj, S., Choudhari, R., Rathi, B., Kumar, D., 2020. Structure-based drug repurposing for targeting Nsp9 replicase and spike proteins of severe acute respiratory syndrome coronavirus 2. J. Biomol. Struct. Dyn. 24, 1–4.

Chauhan, D.S., Yadav, S., Quraishi, M.A., 2021. Natural products as environmentally safe and green approach to combat Covid-19. Curr. Res. Green Sustain. Chem. 4, 100114.

Contou, D., Claudinon, A., Pajot, O., Micaëlo, M., Flandre, P.L., Dubert, M., Cally, R., Logre, E., Fraissé, M., Mentec, H., Plantefève, G., 2020. Bacterial and viral co-infections in patients with severe SARS-CoV-2 pneumonia admitted to a French ICU. Ann. Intensive Care. 10, 1–9.

Dagur, P.K., McCoy Jr, J.P., 2015. Collection, storage, and preparation of human blood cells. Curr. Protoc. Cytom. 73, 5–11.

Deore, A.B., Dhumane, J.R., Wagh, R., Sonawane, R., 2019. The stages of drug discovery and development process. Asian J. Pharm. Res. Dev. 7, 62–67.

Elfiky, A.A., 2021. Natural products may interfere with SARS-CoV-2 attachment to the host cell. J. Biomol. Struct. Dyn. 39, 3194–3203.

Ghareeb, D.A., Saleh, S.R., Seadawy, M.G., Nofal, M.S., Abdulmalek, S.A., Hassan, S.F., Khedr, S.M., AbdElwahab, M.G., Sobhy, A.A., Abdel-Hamid, A.S.A., Yassin, A.M., Elmoneam, A.A.A., Masoud, A.A., Kaddah, M.M.Y., El-Zahaby, S.A., Al-mahallawi, A.M., El-Gharbawy, A.M., Zaki, A., Seif, I.k., Kenawy, M.Y., Amin, M., Amer, K., El Demellawy, M.A., 2021a. Nanoparticles of ZnO/Berberine complex contract COVID-19 and respiratory co-bacterial infection in addition to elimination of hydroxychloroquine toxicity. J. Pharm. Investig. 51 (6), 735–757.

Ghareeb, D.A., Saleh, S.R., Nofal, M.S., Kaddah, M.M.Y., Hassan, S.F., Seif, I.K., El-Zahaby, S.A., Khedr, S.M., Kenawy, M.Y., Masoud, A.A., Soudi, S.A., Sobhy, A.A., Sery, J.G., El-Wahab, M.G.A., Elmoneam, A.A.A., Al-mahallawi, A.M., El-Demellawy, M.A., 2021b. Potential therapeutic and pharmacological strategies for SARS-CoV2. J. Pharm. Investig. 51 (3), 281–296.

Guan, S., Zhu, K., Dong, Y., Li, H., Yang, S., Wang, S., Shan, Y., 2020. Exploration of binding mechanism of a potential streptococcus pneumoniae neuraminidase inhibitor from herbaceous plants by molecular simulation. Int. J. Mol. Sci. 21, 1003–1015.

Hamdi, M., Abdel-Bar, H.M., Elmowafy, E., El-Khouly, A., Mansour, M., Awad, G.A., 2021. Investigating the internalization and COVID-19 antiviral computational analysis of optimized nanoscale zinc oxide. ACS Omega. 6 (10), 6848–6860.

Infante, M., Ricordi, C., Alejandro, R., Caprio, M., Fabbri, A., 2021. Hydroxychloroquine in the COVID-19 pandemic era: in pursuit of a rational use for prophylaxis of SARS-CoV-2 infection. Expert Rev. Anti Infect. Ther. 19 (1), 5–16.

Jack A, Ferro L, Trnka M, Wehri E, Nadgir A, Nguyenla X, et al. 2020. SARS-CoV-2 nucleocapsid protein forms condensates with viral genomic RNA. BioRxiv. doi:10.1101/2020.09, 14, v3.

Kadaikunnan, S., Rejiniemon, T.S., Khaled, J.M., Alharbi, N.S., Mothana, R., 2015. *In-vitro* antibacterial, antifungal, antioxidant and functional properties of *Bacillus amyloliquefaciens*. Ann. Clin. Microbiol. Antimicrob. 14 (1), 9–19.

Kalinowska, M., Sienkiewicz-Gromiuk, J., Świderski, G., Pietryczuk, A., Cudowski, A., Lewandowski, W., 2020. Zn (II) complex of plant phenolic chlorogenic acid: Antioxidant, Antimicrobial and structural studies. Materials. 13, 3745–3762.

Liu, J., Zheng, X., Tong, Q., Li, W., Wang, B., Sutter, K., Trilling, M., Lu, M., Dittmer, U., Yang, D., 2020. Overlapping and discrete aspects of the pathology and pathogenesis of the emerging human pathogenic coronaviruses SARS-CoV, MERS-CoV, and 2019-nCoV. J. Med. Virol. 92 (5), 491–494.

Matei, M.F., Jaiswal, R., Kuhnert, N., 2012. Investigating the chemical changes of chlorogenic acids during coffee brewing: Conjugate addition of water to the

olefinic moiety of chlorogenic acids and their quinides. J. Agric. Food Chem. 60 (49), 12105–12115.
Moon, A., Agrawa, T., Gupta, P., Kondlekar, N., Taksande, A., 2017. Anti-cancer therapy: Chlorogenic acid, gallic acid and ellagic acid in synergism. IOSR J. Pharm. Biol. Sci. 12, 48–52.
Prasad, N.R., Karthikeyan, A., Karthikeyan, S., Reddy, B.V., 2011. Inhibitory effect of caffeic acid on cancer cell proliferation by oxidative mechanism in human HT-1080 fibrosarcoma cell line. Mol. Cel. Biochem. 349 (1), 11–19.
Risch, H.A., 2020. Risch responds to "how to consider low reported death rates in COVID-19". Am. J. Epidemiol. 189, 1230–1231.
Sharma, D., Shandilya, P., Saini, N.K., Singh, P., Thakur, V.K., Saini, R.V., Mittal, D., Chandan, G., Saini, V., Saini, A.K., 2021. Insights into the synthesis and mechanism of green synthesized antimicrobial nanoparticles, answer to the multidrug resistance. Mater. Today Chem. 19.
Shin, D., Mukherjee, R., Grewe, D., Bojkova, D., Baek, K., Bhattacharya, A., Schulz, L., Widera, M., Mehdipour, A.R., Tascher, G., Geurink, pp., 2020. Papain-like protease regulates SARS-CoV-2 viral spread and innate immunity. Nature. 587 (7835), 657–662.
Soto, M.E., Guarner-Lans, V., Soria-Castro, E., Manzano Pech, L., Pérez-Torres, I., 2020. Is antioxidant therapy a useful complementary measure for Covid-19 treatment? An algorithm for its application. Medicina. 56, 386–414.
Tai, W., He, L., Zhang, X., Pu, J., Voronin, D., Jiang, S., Zhou, Y., Du, L., 2020. Characterization of the receptor-binding domain (RBD) of 2019 novel coronavirus: implication for development of RBD protein as a viral attachment inhibitor and vaccine. Cell Mol. Immunol. 17 (6), 613–620.
Walls, A.C., Park, Y.J., Tortorici, M.A., Wall, A., McGuire, A.T., Veesler, D., 2020. Structure, function, and antigenicity of the SARS-CoV-2 spike glycoprotein. Cell. 181 (2), 281–292.
Wan, Y., Shang, J., Graham, R., Baric, R.S., Li, F., Gallagher, T., 2020. Receptor recognition by the novel coronavirus from Wuhan: an analysis based on decade-long structural studies of SARS coronavirus. J. Virol. 94 (7).
Wang, W.-X., Zhang, Y.-R., Luo, S.-Y., Zhang, Y.-S., Zhang, Y.i., Tang, C.e., 2022. Chlorogenic acid, a natural product as potential inhibitor of COVID-19: virtual screening experiment based on network pharmacology and molecular docking. Nat. Prod. Res. 36 (10), 2580–2584.
Weng, J.R., Lin, C.S., Lai, H.C., Lin, Y.P., Wang, C.Y., Tsai, Y.C., Wu, K.C., Huang, S.H., Lin, C.W., 2019. Antiviral activity of *Sambucus Formosana Nakai* ethanol extract and related phenolic acid constituents against human coronavirus NL63. Virus Res. 273, 197767–197774.
Xia, S., Liu, M., Wang, C., Xu, W., Lan, Q., Feng, S., Qi, F., Bao, L., Du, L., Liu, S., Qin, C., 2020. Inhibition of SARS-CoV-2 (previously 2019-nCoV) infection by a highly potent pan-coronavirus fusion inhibitor targeting its spike protein that harbors a high capacity to mediate membrane fusion. Cell Res. 30 (4), 343–355.
Yu, J.W., Wang, L., Bao, L.D., 2020. Exploring the active compounds of traditional Mongolian medicine in intervention of novel coronavirus (COVID-19) based on molecular docking method. J. Funct. Foods. 71, 104016–104025.
Zhu, N.a., Zhang, D., Wang, W., Li, X., Yang, B.o., Song, J., Zhao, X., Huang, B., Shi, W., Lu, R., Niu, P., Zhan, F., Ma, X., Wang, D., Xu, W., Wu, G., Gao, G.F., Tan, W., 2020. A novel coronavirus from patients with pneumonia in China, 2019. N. Engl. J. Med. 382 (8), 727–733.